Inorg. Chem. **2007**, *46*, 10294–10306

Iron(III) Complexes of Tridentate 3N Ligands as Functional Models for Catechol Dioxygenases: The Role of Ligand *N*-alkyl Substitution and Solvent on Reaction Rate and Product Selectivity

Kusalendiran Visvaganesan,[†] Ramasamy Mayilmurugan,[†] Eringathodi Suresh,[‡] and Mallayan Palaniandavar*,[†]

School of Chemistry, Bharathidasan University, Tiruchirappalli-620 024, India, Analytical Science Discipline, Central Salt and Marine Chemicals Research Institute, Bhavnagar-364 002, India

Received April 29, 2007

A series of iron(III) complexes of the type $[Fe(L)Cl_3]$, where L is the variously *N*-alkyl-substituted bis(pyrid-2-ylmethyl)amine ligand such as bis(pyrid-2-ylmethyl)amine (L1), *N*,*N*-bis(pyrid-2-ylmethyl)methylamine (L2), *N*,*N*-bis-(pyrid-2-ylmethyl)-*n*-propylamine (L3), *N*,*N*-bis(pyrid-2-ylmethyl)-*iso*-butylamine (L4), *N*,*N*-bis(pyrid-2-ylmethyl)-*iso*-propylamine (L5), *N*,*N*-bis(pyrid-2-ylmethyl)cyclohexylamine (L6), and *N*,*N*-bis(pyrid-2-ylmethyl)-*tert*-butylamine (L7), have been isolated and characterized by elemental analysis and spectral and electrochemical methods. The crystal structures of the complexes $[Fe(L2)Cl_3]$ **2**, $[Fe(L3)Cl_3]$ **3**, and the complex-substrate adduct $[Fe(L5)(TCC)(NO_3)]$ **5a**, where TCC^{2-} is the tetrachlorocatecholate dianion, have been determined by single-crystal X-ray crystallography. The complexes $[Fe(L2)Cl_3]$ **2** and $[Fe(L3)Cl_3]$ **3** possess a distorted octahedral geometry, in which the linear tridentate 3N ligands are cis-facially coordinated to the iron(III) center, and three chloride ions occupy the remaining coordination sites. The replacement of the *N*-methyl group in **2** by *N*-*n*-propyl group as in **3** leads to the formation of the Fe–N_{py} bonds and also the Fe–Cl bonds located trans to them of different lengths. The catecholate adduct **5a** also possesses a distorted octahedral geometry, in which the ligand is cis-facially coordinated to iron(III) center, TCC^{2-} is asymmetrically chelated trans to the two pyridyl moieties of the ligand, and one of the oxygen atoms of the nitrate ion occupies the sixth coordination site. All of the present complexes have been interacted with simple and substituted catechols. The catecholate adducts [Fe(L)(DBC)Cl] and $[Fe(L)(DBC)(Sol)]^+$, where H_2DBC is 3,5-di-*tert*-butylcatechol and Sol = H_2O/CH_3CN, have been generated in situ, and their spectral and redox properties and dioxygenase activities have been studied in dimethylformamide and dichloromethane solutions. All of the complexes catalyze the cleavage of H_2DBC using molecular oxygen to afford both intra- and extradiol cleavage products. The formation of extradiol cleavage products is facilitated by cis-facial coordination of the 3N ligands and availability of vacant coordination site on iron(III) center for dioxygen binding. It is remarkable that the nature of the *N*-alkyl substituent in 3N ligands controls the regioselectivity of cleavage, with the *n*-propyl, *iso*-butyl, *iso*-propyl, and cyclohexyl groups enhancing the yield of extradiol products (46–68%) in dichloromethane. The rate of oxygenation depends upon the solvent and the Lewis acidity of iron(III) center as modified by the sterically demanding *N*-alkyl groups-length and degree of substitution. The plot of log (k_{O_2}) versus energy of the low-energy DBC^{2-}-to-iron(III) LMCT band is linear, demonstrating the importance of the Lewis acidity of the iron(III) center in dictating the rate of the dioxygenase reaction.

Introduction

The conversion of dihydroxyaromatic compounds into aliphatic products is the more-common pathway for the biodegradation of naturally occurring aromatic pollutants. A number of nonheme enzymes like catechol dioxygenases with active sites containing iron have the metabolic capability to degrade catechols and other dihydroxyaromatic compounds into aliphatic/acyclic products by the insertion of molecular oxygen.[1] Catechol dioxygenase enzymes can be classified into two subclasses, namely, intradiol and extradiol catechol

* To whom correspondence should be addressed. E-mail: palaniandavarm@gmail.com, palanim51@yahoo.com.
[†] Bharathidasan University.
[‡] Central Salt and Marine Chemicals Research Institute.

10.1021/ic700822y CCC: $37.00
Published on Web 10/24/2007

Scheme 1. Mode of Cleavage of Extradiol and Intradiol Dioxygenases

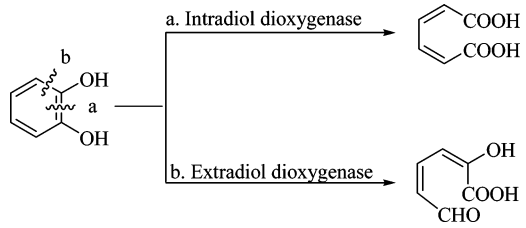

dioxygenases on the basis of regiospecificity of ring cleavage. The former catalyze the cleavage of the carbon−carbon double bond of the enediol moiety utilizing the iron(III) active center, whereas the latter containing the iron(II) active site cleave the carbon−carbon double bond adjacent to the enediol moiety to yield 2-hydroxymuconic semialdehyde as the product (Scheme 1). The iron(III) center in the intradiol-cleaving protocatechuate 3,4-dioxygenase[2] assumes a trigonal bipyramidal active-site geometry ligated by two histidine and two tyrosine amino acid residues and a solvent-derived molecule.[3−5] In contrast, the iron(II) active site in the extradiol dioxygenase enzyme 2,3-dihydroxybiphenyl 1,2-dioxygenase (BphC) possesses a square-pyramidal geometry with a 2-His-1-carboxylate facial-triad structural motif and two water molecules.[6−9]

Even though intradiol dioxygenases and their models[11−21] have been more extensively studied and thus more understood, extradiol dioxygenase enzymes have not been studied in detail, in spite of the latter constituting the more-common iron enzymes for the biodegradation of aromatic molecules in the soil. The difficulty in studying extradiol dioxygenases could be attributed to the lack of spectroscopic probes available for iron(II), and oxygen activation mechanism has been proposed[22] for the extradiol cleavage. Solomon et al. have very recently found that the resting extradiol-cleaving enzymes fail to react with O_2 but become reactive upon substrate binding.[10] In contrast to their intradiol counterparts, model complexes capable of eliciting extradiol cleavage activity are only fewer in number.[23−31] Earlier, Funabiki et al.[24] reported the first model using $FeCl_2/FeCl_3$ with a pyridine/bipyridine mixture. Later, Die et al.[25] found that [Fe(TACN)(DBC)Cl] (TACN = 1,4,7-triazacyclononane), upon exposure to molecular oxygen, yielded 35% of the extradiol product-substituted 2-pyrones. Que et al. and Bugg et al. have studied the reactivity of [Fe(TACN)(DBC)Cl] with molecular oxygen and suggested that cis-facial coordination of the tridentate ligand and both mono- and dianionic catecholate binding lead to extradiol cleavage and that the iron−catecholate adduct must contain a vacant coordination site for oxygen binding.[26−28] Que et al.[28] and Palaniandavar et al.[32] have recently reported that tridentate ligands with meridional coordination yield quinone and intradiol cleavage products as the major products and confirmed that cis-facial coordination of tridentate ligands is essential to elicit extradiol cleavage. On substituting the N−H hydrogen of TACN in [Fe(TACN)(DBC)Cl] with methyl groups as in [Fe(Me_3-TACN)(DBC)Cl], a nearly quantitative yield (97%) of extradiol cleavage product is observed,[28] even without the addition of pyridine. Very recently, Gebbink et al. have isolated the iron(II)- and iron(III)-catecholate complexes of a new family of substituted 3,3-bis(1-alkylimidazol-2-yl)-propionate ligands, and the iron(III) complexes elicit both the extra- and intradiol cleavage products in comparable amounts.[33] All of these studies reveal that the steric and electronic properties of ligands coordinated to iron(III) lead to a dramatic difference in the cleavage preferences between the structurally similar catalysts and that there are subtle factors yet to be identified that modulate the oxidative-cleavage mechanism.

(1) Hayaishi, O.; Katagiri, M.; Rothberg, S. *J. Am. Chem. Soc.* **1955**, *77*, 5450.
(2) Ohlenddorf, D. H.; Lipscomb, J. D.; Weber, P. C. *Nature* **1988**, *336*, 403.
(3) Ohlenddorf, D. H.; Orville, A. M.; Lipscomb, J. D. *J. Mol. Biol.* **1994**, *244*, 586.
(4) Vetting, M. W.; Earhart, C. A.; Ohlenddorf, D. H. *J. Mol. Biol.* **1994**, *236*, 372.
(5) Pau, M. Y. M.; Davis, M. I.; Orville, A. M.; Lipscomb, J. D.; Solomon, E. I. *J. Am. Chem. Soc.* **2007**, *129*, 1944.
(6) Han, S.; Eltis, L. D.; Timmis, K. N.; Muchmore, S. W.; Bolin, J. T. *Science* **1995**, *270*, 976.
(7) Kita, A.; Kita, S. I.; Fujisawa, I.; Inaka, K.; Ishida, T.; Horiike, K.; Nozaki, M.; Miki, K. *Structure* **1998**, *7*, 25.
(8) Sugimoto, K.; Senda, T.; Aoshima, H.; Masai, E.; Fukuda, M.; Mitsui, Y. *Structure* **1999**, *7*, 953.
(9) Titus, G. P.; Mueller, H. A.; Burgner, J.; Rodriguez de Cordoba, S.; Penalva, M. A.; Timm, D. E. *Nature Struct. Biol.* ***2000****, 7, 542.*
(10) Davis, M. I.; Wasinger, E. C.; Decker, A.; Pau, M. Y. M.; Vaillancourt, F. H.; Bolin, J. T.; Eltis, L. D.; Hedman, B.; Hodgson, K. O.; Solomon, E. I. *J. Am. Chem. Soc.* **2003**, *125*, 11214.
(11) Viswanathan, R.; Palaniandavar, M.; Balasubramanian, T.; Muthiah, P. T. *J. Chem. Soc., Dalton. Trans.* **1996**, *2519.*
(12) Viswanathan, R.; Palaniandavar, M.; Balasubramanian, T.; Muthiah, P. T. *Inorg. Chem.* **1998**, *37*, 2943.
(13) Velusamy, M.; Palaniandavar, M.; Srinivasagopalan, R.; Kulkarni, G. U. *Inorg. Chem.* **2003**, *42*, 8283.
(14) Velusamy, M.; Mayilmurugan, R.; Palaniandavar, M. *Inorg. Chem.* **2004**, *43*, 6284.
(15) Velusamy, M.; Mayilmurugan, R.; Palaniandavar, M. *J. Inorg. Biochem.* **2005**, *99*, 1032.
(16) Pascaly, M.; Duda, M.; Schweppe, F.; Zurlinden, K.; Muller, F. K.; Krebs, B. *J. Chem. Soc., Dalton Trans.* **2001**, 828.
(17) Ogo, S.; Yamahara, R.; Funabiki, T.; Masuda, H.; Watanabe, Y. *Chem. Lett.* **2001**, 1062.
(18) Cox, D. D.; Que, L., Jr. *J. Am. Chem. Soc.* **1988**, *110*, 8085.
(19) Jang, H. G.; Cox, D. D.; Que, L., Jr. *J. Am. Chem. Soc.* **1991**, *113*, 9200.
(20) Koch, W. O.; Schünemann, V.; Gerdan, M.; Trautwein, A. X.; Krüger, H. J. *Chem.—Eur. J.* **1998**, *4*, 1255.
(21) Raffard, N.; Carina, R.; Simaan, A. J.; Sainton, J.; Riviere, E.; Tchertanov, L.; Bourcier, S.; Bouchoux, G.; Delroisse, M.; Banse, F.; Girerd, J. J. *Eur. J. Inorg. Chem.* **2001**, 2249.
(22) Shu, L.; Chiou, Y. M.; Orville, A, M.; Miller, M. A.; Lipscomb, J. D.; Que, L., Jr. *Biochemistry* **1995**, *34*, 6649.
(23) Costas, M.; Mehn, M. P.; Jensen, M. P.; Que, L., Jr. *Chem. Rev.* **2004**, *104*, 939.
(24) Funabiki, T.; Mizoguchi, A.; Sugimoto, T.; Tada, S.; Tsugi, M.; Sakamoto, H.; Yoshida, S. *J. Am. Chem. Soc.* **1986**, *108*, 2921.
(25) Dei, A.; Gatteschi, D.; Pardi, L. *Inorg. Chem.* **1993**, *32*, 1389.
(26) Lin, G.; Reid, G.; Bugg, T. D. H. *J. Am. Chem. Soc.* **2001**, *123*, 5030.
(27) Ito, M.; Que, L., Jr. *Angew. Chem., Int. Ed. Engl*. **1997**, *36*, 1342.
(28) Jo, D.-H.; Que, L., Jr. *Angew. Chem., Int. Ed.* **2000**, *39*, 4284.
(29) Lim, J. H.; Park, T. H.; Lee, H.-J.; Lee, K.-B.; Jang, H. G. *Bull. Korean Chem. Soc.* **1999**, *20*, 1428.
(30) Chiou, Y.-M.; Que, L., Jr. *Inorg. Chem.* **1995**, *34*, 3577.
(31) Mayilmurugan, R.; Suresh, E.; Palaniandavar, M. *Inorg. Chem.* **2007**, *46*, 6038.
(32) Dhanalakshmi, T.; Bhuvaneshwari, M.; Palaniandavar, M. *J. Inorg. Biochem.* **2006**, *100*, 1527.
(33) Bruijnincx, P. C. A.; Lutz, M.; Spek, A. L.; Hagen, W. R.; Weckhuysen, B. M.; Koten, G.; Klein Gebbink, R. J. M. *J. Am. Chem. Soc.* **2007**, *129*, 2275.

Scheme 2. Tridentate 3N Ligands and Their cis-Facial Coordination in $[Fe(L)Cl_3]$ (a) and $[Fe(L)(DBC)(X)]$ (b) Complexes

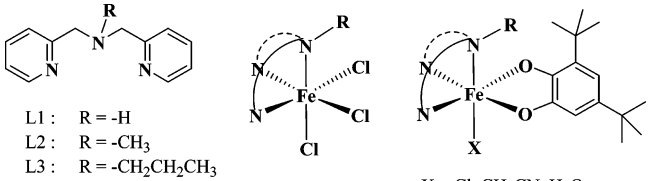

Scheme 3. Structures of Catechols Used in This Study

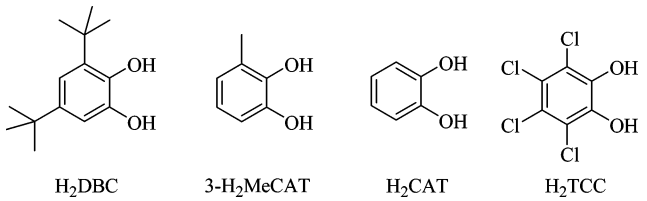

In our laboratory, we had investigated 1:1 iron(III) complexes of several linear 3N[15] and 2NO[32] ligands with an aim to mimic the extradiol-cleaving enzymes and correlate the reaction rate as well as extradiol cleavage yields of the model complexes with the ligand environment (steric and electronic demand). Complex $[Fe(L1)Cl_3]$, where L1 is bis-(pyrid-2-ylmethyl)amine (Scheme 2), possesses a cis-facial coordination of the 3N ligand but catalyzes the intradiol cleavage of catechols.[15] On the other hand, the iron(III) complexes of *N*,*N*-bis(pyrid-2-ylmethyl)benzylamine[28] and bis(benzimidazol-2-ylmethyl)amine,[34] yield respectively 72 and 60% extradiol cleavage products. So, in this study we have isolated iron(III) complexes of a series of linear *N*-alkyl-substituted bis(pyrid-2-ylmethyl)amine ligands to understand the role of ligand steric and electronic factors on iron(III) coordination geometry by systematically varying the *N*-alkyl groups. The pyridine moieties in the ligands would mimic the histidine residues, and the ligands are expected to impose a facial coordination upon iron(III), which is reminiscent of the cis-facial structural motif in the extradiol-cleaving enzymes. Also, we intend to study the interaction of the complexes with variously substituted catechols (Scheme 3) to understand the dioxygenase activity and thus probe the importance of the facial topology and the *N*-alkyl substituent in eliciting extradiol cleavage. The single-crystal X-ray structures of $[Fe(L2)Cl_3]$ and $[Fe(L3)Cl_3]$ have been obtained to show that in all of these complexes the 3N ligands are cis-facially coordinated and labile sites are available for coordination of the substrate catechol. The catecholate adduct $[Fe(L5)(TCC)(NO_3)]$ has structural features relevant to that of the ternary substrate adduct of the enzyme BphC in which the sixth coordination site is occupied by NO.[35] Also, we have found that almost all of the present complexes elicit extradiol cleavage in dichloromethane solvent and that the nature of the *N*-alkyl group in the ligands tunes the selectivity in the extradiol cleavage products.

Experimental Section

Materials. 3,4,5,6-Tetrachlorocatechol (Lancaster), pyridine-2-carboxaldehyde, *n*-propylamine, *iso*-propylamine, *tert*-butylamine, *iso*-butylamine, cyclohexylamine, 3,5-di-*tert*-butylcatechol, $AgClO_4 \cdot H_2O$, iron(III) nitrate nonahydrate, sodium triacetoxyborohydride, bis(pyrid-2-ylmethyl)amine (L1) (Aldrich), 3-methylcatechol (Acros), sodium hydride, catechol (Loba, India), anhydrous iron(III) chloride, aqueous formaldehyde (37%), triethylamine, *N*,*N*-dimethylformamide, dichloromethane, tetrahydrofuran, ethylacetate, and *n*-hexane (Merck, India) were used as received. The supporting electrolyte tetrabutylammonium perchlorate (TBAP) was prepared in water and recrystallized twice from aqueous ethanol. Methanol and acetonitrile were distilled before use.

Synthesis of Ligands. *N*,*N*-Bis(pyrid-2-ylmethyl)methylamine (L2). This was prepared by a method reported previously.[36]

Reductive Amination. A General Procedure. A common procedure was followed to prepare all of the other ligands L3−L7.[37] To a mixture of (4.5 mmol) alkylamine and sodium triacetoxyborohydride (3.75 g, 17.7 mmol) in dichloromethane (100 mL) was added pyridine-2-carboxaldehyde (1.45 g, 13.5 mmol) and stirred for 18 h. The reaction was quenched with saturated sodium hydrogencarbonate and extracted with ethylacetate (3 × 150 mL). The organic fractions were combined, dried (Na_2SO_4), and the solvent was removed under reduced pressure. The residue was redissolved in tetrahydrofuran (50 mL) and treated with NaH (0.22 g, 9.1 mmol). After the mixture was stirred for 2 h, the solvent was removed and the residue was extracted with dichloromethane. The extracts were combined, and the solvent was evaporated under reduced pressure to obtain the product.

***N*,*N*-Bis(pyrid-2-ylmethyl)-*n*-propylamine (L3).** The above general procedure was followed, and *n*-propylamine was used to obtain L3 as a yellow oil, which is used without further purification. Yield: 1.01 g (83%). ^{1}H NMR (200 MHz, $CDCl_3$): δ 8.54−7.36 (m, 8H), 3.91 (s, 4H), 2.28 (t, 2H), 1.32 (m, 2H), 1.11 (t, 3H). EI-MS m/z = 241 $C_{15}H_{19}N_3^+$.

***N*,*N*-Bis(pyrid-2-ylmethyl)-*iso*-butylamine (L4).** The general procedure described above was followed, and *iso*-butylamine was used to give L4 as a colorless semisolid. Yield: 1.01 g (79%). ^{1}H NMR (200 MHz, $CDCl_3$): δ 8.48−7.29 (m, 8H), 3.88 (s, 4H), 2.38 (d, 2H), 1.87 (m, 1H), 1.05 (d, 6H). EI-MS m/z = 255 $C_{16}H_{21}N_3^+$.

***N*,*N*-Bis(pyrid-2-ylmethyl)-*iso*-propylamine (L5).** The above general procedure was followed, and *iso*-propylamine was used to give L5 as viscous pale-yellow oil, which is used for complex preparation without further purification. Yield: 0.88 g (73%). ^{1}H NMR (200 MHz, $CDCl_3$): δ 8.44−7.26 (m, 8H), 3.81 (s, 4H), 2.31 (m, 1H), 1.01 (d, 6H). EI-MS m/z = 241 $C_{15}H_{19}N_3^+$.

***N*,*N*-Bis(pyrid-2-ylmethyl)cyclohexylamine (L6).** The above general procedure was followed, and cyclohexylamine was used to obtain L6 as colorless prisms. Yield: 1.29 g (92%). ^{1}H NMR (200 MHz, $CDCl_3$): δ 8.49−7.33 (m, 8H), 3.73 (s, 4H), 2.58 (m, 1H), 1.52 (m, 4H), 1.36 (m, 6H). EI-MS m/z = 281 $C_{18}H_{23}N_3^+$.

***N*,*N*-Bis(pyrid-2-ylmethyl)-*tert*-butylamine (L7).** The general procedure described above was followed, and *tert*-butylamine was used to obtain L7 as a white solid. Yield: 1.12 g (88%). ^{1}H NMR

(34) Yoon, S.; Lee, H. J.; Lee, K. B.; Jang, H. G. *Bull. Korean Chem. Soc.* **2000**, *21*, 923.
(35) Arciero, D. M.; Orville, A. M.; Lipscomb, J. D. *J. Biol. Chem.* **1985**, *260*, 14035.
(36) Britovsek, G. J. P.; England, J.; White, A. J. P. *Dalton Tans.* **2006**, 1399.
(37) Britovsek, G. J. P.; England, J.; White, A. J. P. *Inorg. Chem.* **2005**, *44*, 8125.

(200 MHz, $CDCl_3$): δ 8.42−7.22 (m, 8H), 3.81 (s, 4H), 1.12 (s, 9H). EI-MS $m/z = 255$ $C_{16}H_{21}N_3^+$.

Synthesis of Iron(III) Complexes. [Fe(L1)Cl$_3$] (1). [Fe(L1)Cl_3] **1** was prepared as reported earlier[15] by adding $FeCl_3$ (0.16 g, 1 mmol) in methanol (10 mL) to a solution of L1 (0.20 g, 1 mmol) in dry methanol (10 mL), stirred for 30 min, and then cooled. The yellow-colored complex was filtered off, washed with cold methanol and diethylether, and then dried under vacuum.

[Fe(L2)Cl$_3$] (2). This compound was prepared using the procedure reported in the literature.[38] Single crystals suitable for X-ray diffraction were obtained by the slow evaporation of an acetonitrile solution of the complex. Yield: 0.26 g (69%). Anal. Calcd for $C_{13}H_{15}Cl_3FeN_3$: C, 41.58; H, 4.03; N, 11.19. Found: C, 41.35; H, 4.11; N, 11.32%.

[Fe(L3)Cl$_3$] (3). This complex was prepared in a manner analogous to that described for **1** using L3 instead of L1. The yellow needles of X-ray quality crystals were obtained by vapor diffusion of diethylether into an acetonitrile solution of the complex. Yield: 0.30 g (75%) Anal. Calcd for $C_{15}H_{19}Cl_3FeN_3$: C, 44.65; H, 4.75; N, 10.41. Found: C, 44.25; H, 4.81; N, 10.32%.

[Fe(L4)Cl$_3$] (4). 4 was also prepared using the procedure employed for isolating [Fe(L1)Cl_3]. Yield: 0.33 g (78%) Anal. Calcd for $C_{16}H_{21}Cl_3FeN_3$: C, 46.02; H, 5.07; N, 10.06. Found: C, 46.05; H, 4.96; N, 10.12%. ESI-MS $m/z = 382$ $[Fe(L4)Cl_2]^+$.

[Fe(L5)Cl$_3$] (5). This complex was prepared using the procedure adopted for obtaining [Fe(L1)Cl_3]. Yield: 0.30 g (73%) Anal. Calcd for $C_{15}H_{19}Cl_3FeN_3$: C, 44.65; H, 4.75; N, 10.41. Found C, 44.72; H, 4.69; N, 10.40%.

[Fe(L6)Cl$_3$] (6). This complex was prepared as a dark-yellow colored product using the procedure employed for preparing [Fe(L1)Cl_3]. Yield: 0.38 g (85%) Anal. Calcd for $C_{18}H_{23}Cl_3FeN_3$: C, 48.74; H, 5.23; N, 9.47. Found: C, 48.65; H, 5.31; N, 9.53%. ESI-MS, $m/z = 408$ $[Fe(L6)Cl_2]^+$.

[Fe(L7)Cl$_3$] (7). 7 was prepared using the procedure adopted for isolating [Fe(L1)Cl_3]. Yield: 0.34 g (82%) Anal. Calcd for $C_{16}H_{21}Cl_3FeN_3$: C, 46.02; H, 5.07; N, 10.06. Found C, 47.08; H, 5.02; N, 10.04%. ESI-MS, $m/z = 382$ $[Fe(L7)Cl_2]^+$.

[Fe(L5)(TCC)(NO$_3$)]·0.5C$_3$H$_6$O (5a). An ethanol/acetone (3:2 v/v) solution (2 mL) of $Fe(NO_3)_3 \cdot 9H_2O$ (40.4 mg, 0.1 mmol) was added to L5 (24.1 mg, 0.1 mmol), dissolved in the same solvent (2 mL), and then heated in a water bath. To this hot solution was then added 3,4,5,6-tetrachlorochlorocatechol (24.8 mg, 0.1 mmol) and piperidine (8.5 mg, 20 μL, 0.2 mmol) dissolved in the same solvent. The mixture was refluxed for a few minutes. Dark-purple crystals of the adduct were formed within a few days upon slow cooling and standing and were suitable for X-ray diffraction. Yield: 53.2 mg (84%) Anal. Calcd for $C_{21}H_{19}Cl_4FeN_4O_5 \cdot 0.5C_3H_6O$: C, 42.62; H, 3.50; N, 8.84. Found C, 41.98; H, 3.76; N, 9.04.

Physical Measurements. Elemental analyses were performed on a PerkinElmer Series II CHNS/O analyzer 2400. The electronic spectra were recorded on an Agilent 8453 diode array spectrophotometer. ^{1}H NMR spectra were recorded on a Bruker 200 MHz NMR spectrometer. Mass spectrometry was performed on a QTOF ESI-MS spectrometer. Cyclic voltammetry and differential pulse voltammetry were performed at 25.0 ± 0.2 °C using a three-electrode cell configuration. A platinum sphere, a platinum plate, and Ag(s)/$AgNO_3$ were used as working, auxiliary, and reference electrodes, respectively. The Ag(s)/Ag^+ reference electrode consists of a silver wire immersed in a solution of $AgNO_3$ (0.01 M) and tetrabutylammonium perchlorate (0.1 M) in acetonitrile placed in a tube fitted with a vycor plug. The instruments utilized included an EG & G PAR 273 potentiostat/galvanostat and P−IV computer, along with EG & G M270 software to carry out the experiments and to acquire the data. The temperature of the electrochemical cell was maintained by a cryocirculator (HAAKE D8-G). The $E_{1/2}$ observed under identical conditions for the Fc/Fc^+ couple in acetonitrile was 0.100 V with respect to the Ag(s)/Ag^+ reference electrode. The experimental solutions were deoxygenated by bubbling research-grade nitrogen, and an atmosphere of nitrogen was maintained over the solution during measurement. The products were analyzed using a Hewlett-Packard (HP) 6890 Gas Chromatograph (GC) series equipped with a flame ionization detector (FID) and a HP-5 capillary column (30 m × 0.32 mm × 2.5 μm). A GC-MS analysis was performed on a PerkinElmer Clarus 500 GC-MS (Electron Ionization) instrument using a PE-5 (HP-5 equiv) capillary column.

Table 1. Crystal Data and Structure Refinement for [Fe(L2)Cl_3] **2**, [Fe(L3)Cl_3] **3** and [Fe(L5)(TCC)(NO_3)]·0.5C_3H_6O **5a**

	2	**3**	**5a**
empirical formula	$C_{13}H_{15}Cl_3FeN_3$	$C_{15}H_{15}Cl_3FeN_3$	$C_{45}H_{44}Cl_8Fe_2N_8O_{11}$
fw	375.49	399.51	1268.20
cryst syst	orthorhombic	monoclinic	monoclinic
space group	*Pnma*	*P*21/*n*	C2/*c*
a (Å)	14.0080(9)	11.7917(13)	26.424(10)
b (Å)	14.5023(9)	11.6295(13)	13.426(5)
c (Å)	7.4663(5)	14.0247(15)	17.042(7)
α (deg)	90	90	90
β (deg)	90	114.309(2)	117.496(7)
γ (deg)	90	90	90
V (Å^3)	1516.77(17)	1752.7(3)	5363(4)
Z	4	4	4
ρ_{calcd} (g/cm^3)	1.644	1.514	1.571
F(000)	764	812	2584
T (K)	273	273	293
radiation [Mo Kα] (Å)	0.71073	0.71073	0.71073
residuals [$I > 2\sigma(I)$]			
R1[a]	0.0215	0.0623	0.0699
wR2[b]	0.0587	0.1292	0.1524

[a] $R1 = [\sum(||F_o| - |F_c||)/\sum|F_o|]$. [b] $wR2 = \{[\sum(w(F_o^2 - F_c^2)^2)/\sum(wF_o^4)]^{1/2}\}$.

Crystallographic Refinement and Structure Solution. A crystal of suitable size selected from the mother liquor was immersed in paraffin oil, then mounted on the tip of a glass fiber and cemented using epoxy resin. Intensity data for the crystals were collected using Mo Kα ($\lambda = 0.71073$ Å) radiation on a Bruker SMART APEX diffractometer equipped with a CCD area detector at 273 and 293 K. The crystallographic data were collected in Table 1. The *SMART*[39] program was used for collecting frames of data, indexing the reflections, and determination of lattice parameters; *SAINT*[39] program for integration of the intensity of reflections and scaling; *SADABS*[40] program for absorption correction, and the *SHELXTL*[41] program for space group and structure determination and least-squares refinements on F^2. The structure was solved by the heavy-atom method. Other non-hydrogen atoms were located in successive difference Fourier syntheses. The final refinement was performed by full-matrix least-squares analysis. Hydrogen atoms attached to the ligand moiety were located from the difference Fourier map and refined isotropically.

Characterization of Oxygenation Products. The three major cleavage products **9**, **11**, and **13** were isolated by column chroma-

(38) Mukherjee, J.; Balamurugan, V.; Gupta, R.; Mukherjee, R. *Dalton Trans.* **2003**, 3686.

(39) *SMART & SAINT Software Reference manuals*, version 5.0; Bruker AXS Inc.: Madison, WI, 1998.

(40) Sheldrick, G. M. *SADABS Software for Empirical Absorption Correction*; University of Göttingen: Göttingen, Germany, 2000.

(41) *SHELXTL Reference Manual*, version 5.1; Bruker AXS Inc.: Madison, WI, 1998.

tography over silica gel (60−120 mess) using 5−10% ethylacetate in *n*-hexane and identified using retention times of GC-MS (EI) and ^{1}H NMR spectroscopy. The other three minor products **8**, **10**, and **12** were analyzed as a mixture and identified by GC-MS (EI) analysis. The regioisomers **8**/**10** and **9**/**11** were distinguished by comparison of their retention times of GC (FID) and GC-MS (EI) and the intensity of the fragmentation pattern in the mass spectrum. All of the products were quantified using GC (FID) with the following temperature program: injector temperature 130 °C; initial temperature 60 °C, heating rate 10 °C min^{-1} to 130 °C, then increasing at a rate of 2 °C min^{-1} to 160 °C, and then increasing at a rate of 5 °C min^{-1} to 260 °C; FID temperature 280 °C. GC-MS analysis was performed under conditions identical to those used for GC analysis; retention times in GC-MS (EI): 14.6 min for **11**, 15.9 min for **8**, 16.4 min for **9**, 18.1 min for **10**, 19.9 min for **12**, and 21.2 min for **13**. Spectroscopic data are as follows:

3,5-di-*tert*-butyl-2-pyrone (9): GC-MS data found for $C_{13}H_{20}O_2$, m/z = 208 (M^+). ^{1}H NMR ($CDCl_3$): 1.18 (s, 9H), 1.35 (s, 9H), 7.08 (d, 1H), 7.14 (d, 1H).

4,6-di-*tert*-butyl-2-pyrone (11): GC-MS data found for $C_{13}H_{20}O_2$, m/z = 208 (M^+). ^{1}H NMR ($CDCl_3$): 1.19 (s, 9H), 1.26 (s, 9H), 6.04 (d, 1H), 6.14 (d, 1H).

3,5-di-*tert*-butyl-5-(carboxymethyl)-2-furanone (13): GC-MS data found for $C_{14}H_{22}O_4$, m/z = 254 (M^+). ^{1}H NMR ($CDCl_3$): 1.02 (s, 9H), 1.23 (s, 9H), 2.83 (dd, 2H), 6.88 (s, 1H), 9.75 (s).

4,6-di-*tert*-butyloxepine-2,3-dione (8): GC-MS data found for $C_{14}H_{20}O_3$, m/z = 236 (M^+).

5,7-di-*tert*-butyloxepine-2,3-dione (10): GC-MS data found for $C_{14}H_{20}O_3$, m/z = 236 (M^+).

3,5-di-*tert*-butyl-1-oxacyclohepta-3,5-diene-2,7-dione (12): GC-MS data found for $C_{14}H_{20}O_3$, m/z = 236 (M^+).

Reactivity Studies. The catechol cleavage activity of all of the complexes toward H_2DBC was examined by exposing a solution of an iron(III)-DBC^{2-} adduct generated in situ in dimethylformamide (DMF) and dichloromethane (DCM) to molecular oxygen. Kinetic analyses of the catechol cleavage reactions were carried out by time-dependent measurement of the disappearance of the lower-energy DBC^{2-}-to-iron(III) LMCT band in the presence and absence of chloride ions. Silver perchlorate monohydrate dissolved in acetonitrile was used to remove chloride ions from the complex. Stock solutions (6.0×10^{-3} M) of the adducts [Fe(L)(DBC)(Cl)] and [Fe(L)(DBC)(Sol)]$^+$ were prepared by treating [Fe(L)Cl_3] and [Fe(L)(Sol)$_3$]$^{3+}$ complexes ([Fe(L)(Sol)$_3$]$^{3+}$ was prepared by treating [Fe(L)Cl_3] with 3 equiv of $AgClO_4 \cdot H_2O$ in acetonitrile and centrifuging the solution to remove AgCl) with an equiv of H_2DBC pretreated with 2 equiv of Et_3N. The oxygenation reaction was started by rapid delivery of a stock solution (0.2 mL) of the catecholate adducts (6.0×10^{-3} M) by syringe into an O_2-saturated solvent (2.8 mL). The solubilities of O_2 in DMF[42] and in DCM[43] at 25 °C were taken as 4.86 and 5.80 mM, respectively. The product analysis was carried out by stirring the [Fe(L)(Sol)$_3$]$^{3+}$ (0.1 mmol), H_2DBC (0.1 mmol), and triethylamine (0.2 mmol) in dichloromethane (20 mL) solvent under molecular oxygen over 4 h at room temperature. After the reaction was complete, the reaction mixture was concentrated under reduced pressure and extracted with diethylether (3 × 5 mL). The remaining residue was acidified with HCl to pH 3 to decompose the metal complexes and extracted with diethylether (3 × 5 mL). The combined extracts were dried over Na_2SO_4 and then concentrated.

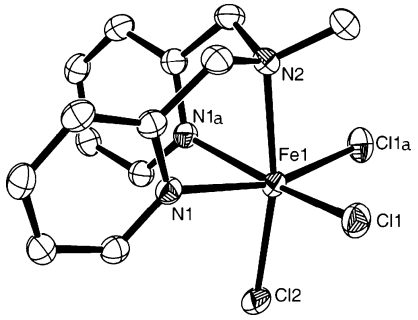

Figure 1. ORTEP diagram of **2** showing 60% probability thermal ellipsoids and the labeling scheme for selected atoms. All of the hydrogen atoms are omitted for clarity.

Results and Discussion

Synthesis of Ligands and Iron(III) Complexes. The linear tridentate 3N ligands L1−L7 (Scheme 2) were synthesized according to known procedures,[37,38] which involve Mannich-base condensation and reductive amination. The hydrogen atom of the −NH group of bis(pyrid-2-ylmethyl)amine has been substituted with different alkyl groups to give differently *N*-alkyl-substituted 3N ligands. The ligand L2 was synthesized from L1 by reductive amination of formaldehyde. All of the other ligands were prepared by reductive amination of the pyridine-2-carboxaldehyde and differently substituted primary amines, using sodium triacetoxyborohydride as the reducing agent.[37] The ligands were reacted with equimolar amounts of $FeCl_3$ in methanol to obtain mononuclear iron(III) complexes in good yields. All of the complexes are formulated as [Fe(L)Cl_3] on the basis of elemental analysis, which is supported by the X-ray crystal structures of **1**,[44] **2**, and **3.** The different *N*-alkyl groups on the ligands are expected to impose varying steric and electronic effects on the iron(III) center. Conductivity studies (Λ_M, 5.2−7.9 $\Omega^{-1}cm^2mol^{-1}$) in dichloromethane (DCM) solution suggest that the chloride ions in all of the complexes remain coordinated to the iron(III) center. However, in DMF solution (Λ_M, 90−120 $\Omega^{-1}cm^2mol^{-1}$) one of the chloride ions is not coordinated.

Description of Structures of [Fe(L2)Cl_3] 2, [Fe(L3)Cl_3] 3, and [Fe(L5)(TCC)(NO_3)] 5a. The X-ray crystal structures of **2** and **3** are shown in Figures 1 and 2, respectively, and the selected bond lengths and bond angles are listed in Table 2. The iron(III) center in **2** is six-coordinate, and the deviation of bond angles at the iron(III) center from ideal angles of 90 and 180° indicate a distorted octahedral coordination geometry. The three nitrogen donor atoms (N1, N1a, and N2) of L2 are coordinated to the iron(III) center in a cis-facial arrangement, and the remaining coordination sites are occupied by three chloride ions. The complex possesses a crystallographic plane of symmetry passing through Cl2, Fe1, N2, and C7 atoms. This illustrates that the two Fe−N_{py} bond lengths [2.194(11) and 2.194(11) Å] and the two Fe−Cl bond lengths [2.311(4) and 2.311(4) Å] trans to the pyridyl moieties are equal. The Fe−N_{amine} bond distance [2.241(16) Å] is longer than the Fe−N_{py} bond lengths due to sp^3 and

(42) Kagaku-Binran Basic, Part II, 2nd ed.; Japan Chemical Society; Tokyo, Japan, 1975.
(43) Pavlova, S. V.; To, H. L.; Chan, E. S. H.; Li, H. W.; Mak, T. C. W.; Lee, H. K.; Chan, S. I. *Dalton Trans.* **2006**, 2232.
(44) Thomas, K. R. J.; Velusamy, M.; Palaniandavar, P. *Acta Crystallogr.* **1998**, *C54*, 741.

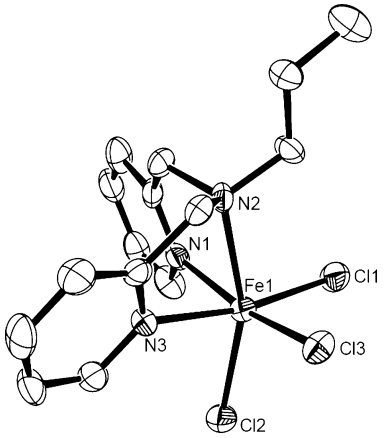

Figure 2. ORTEP diagram of **3** showing 50% probability thermal ellipsoids and the labeling scheme for selected atoms. All of the hydrogen atoms are omitted for clarity.

sp^2 hybridization, respectively, of the amine and pyridine nitrogen atoms.[15,44,45,47] Both of the Fe−Cl bonds [2.311(4) Å] trans to the Fe−N_{py} bonds are longer than the Fe−Cl bond [2.272(5) Å] trans to the Fe−N_{amine} bond, obviously due to the trans effect exerted by the pyridyl moieties. So, Cl1 and Cl1a are more labile than Cl2 and, hence, are expected to be displaced upon catechol binding. The cis-facial coordination of L2 is similar to that of L1 in [Fe(L1)-Cl_3][44] and that of *N*-alkyl-substituted bis(pyrid-2-ylmethyl)-amine ligands in 1:1 iron(III) complexes.[44−47] The Fe−N_{amine} bond in **2** is significantly longer than that in **1**.[44] Obviously, the lone-pair orbital on the nitrogen atom of the sterically hindering *N*-methyl group is not oriented exactly toward the iron(III) orbital, rendering the Fe−N_{amine} bond longer. This illustrates the importance of the steric rather than the electron-releasing effect of the methyl group in dictating the coordination environment around iron(III). A similar elongation in bond length has been observed upon incorporating bulky *N*-alkyl groups in certain [Fe(L)Cl_3] complexes, where L = ((2-bromopyridyl)methyl)bis(pyrid-2-ylmethyl)amine,[46] (((2-p-methoxyphenyl)pyridyl)methyl)bis(pyrid-2-ylmethyl)-amine,[46] and methyl(bis(pyrid-2-yl methyl)amino)acetate.[45]

Similar to **2**, complex **3** also has a distorted octahedral geometry with cis-facial coordination of L3, and the three chloride ions occupy the remaining octahedral coordination sites. Interestingly, there is a significant distortion away from the mirror-plane symmetry observed in the structure of **2**, which is likely caused by the orientation of the bulkier *N*-*n*-propyl group.[46] That the Fe−N_{py} bonds [Fe−N1, 2.176(4); Fe−N3, 2.203(4) Å] are different and that the two Fe−Cl bonds [Fe−Cl1, 2.288(13); Fe−Cl3, 2.303(13) Å] trans to them also become unequal in length is consistent with the structural trans effect. Also, the Fe−N_{amine} bond [2.259(3) Å] is longer than that in **2** due to the enhanced steric demand by the *N*-*n*-propyl group. The Fe−Cl2 bond [2.320(12) Å] trans to the Fe−N_{amine} bond is longer than the Fe−Cl3 bond [2.303(13) Å] and is significantly longer than the Fe−Cl1 bond [2.288(12) Å]. This suggests that Cl2 and Cl3 are more labile than Cl1, which are possibly replaced by catechol during the oxygenation reaction. On the basis of similarities in their spectral behavior (cf. below) **4**−**7** are suggested to display cis-facial coordination of the 3N ligands as in **2** and **3**.

The molecular structure of purple-blue colored **5a** is shown in Figure 3, and the selected bond lengths and bond angles are given in Table 2. The iron(III) center in the complex molecule has a distorted octahedral coordination environment with cis-facial coordination of L5, and the two oxygen atoms of the tetrachlorocatecholate dianion (TCC^{2-}) and one of the oxygen atoms of the nitrate anion occupy the remaining three octahedral coordination sites. The Fe−N_{py} bonds [Fe−N1, 2.139(6); Fe−N3, 2.172(6) Å] are different in length, which is obviously due to the orientation of the sterically hindering *N*-*iso*-propyl. Consequently, the Fe−O_{cat} bonds [Fe−O1, 1.963(5); Fe−O2, 1.933(5) Å] trans to them also become different in length and are longer than those in the TCC^2 adducts of iron(III) complexes of tri-[28,48] and tertadentate[16,48−53] ligands. A similar difference in Fe−O_{cat} bond lengths (0.03 Å) and N_{amine}−Fe−O_{cat} bond angles (13°) have been observed for the analogues complex [Fe(2-BrTPA)(TCC)(NO_3)], where 2-BrTPA is ((2-bromopyridyl)methyl)bis-(pyrid-2-ylmethyl)amine,[55] on account of the orientation of 2-bromopyrid-6-ylmethyl group. The Fe−O−C bond angles (113.2, 112.2°) are slightly higher than those (110.0−112.9°) observed for the TCC^2− adducts of iron(III) complexes of certain tridentate 3N[53] and tripodal 4N ligands.[16,50] We have observed similar enhancement in Fe−O−C bond angles upon incorporating the sterically hindering −NMe_2 group in iron-(III) complexes of certain tripodal tetradentate monophenolate ligands.[14] The cis-facial coordination of L5 in **5a** is similar to the 2-His-1-carboxylate structural motif found in the active sites of the BphC enzyme and the ternary NO adduct of the BphC enzyme−substrate complex. Also, the coordination of one of the oxygen atoms of the nitrate ion in **5a** is similar to that of NO (oxygen surrogate) in the enzyme−substrate adduct, and molecular oxygen is expected to bind at the position occupied by the nitrate ion (cf. below). Further, the difference (0.03 Å) in Fe^{III}−O_{cat} bonds in **5a** with dianionic catechol binding is much lower than that (0.2−0.4 Å) observed in the Fe^{III}−O_{cat} bonds of the BphC enzyme−substrate complex, reflecting the monoanionic coordination of catechol in the latter. However, it is to be noted that the ligand trans effect alone is not enough to

(45) Rodriguez, M. C.; Lambert, F.; Morgenstern-Badarau, I.; Cesario, M.; Guilhem, J.; Keita, B.; Nadjo, L. *Inorg. Chem.* **1997**, *36*, 3525.
(46) Mandon, D.; Nopper, A.; Litrol, T.; Goetz, S. *Inorg. Chem.* **2001**, *40*, 4803.
(47) Stefen, D.; Armin, W.; Ursel, W.; Friedrich, W.; Gerhard, G. *Z. Naturforsch., B: Chem. Sci.* **1997**, *52*, 372.
(48) Ogihara, T.; Hikichi, S.; Akita, M.; Moro-oka, Y. *Inorg. Chem.* **1998**, *37*, 2614.
(49) Jo, D.-H.; Chiou, Y.-M.; Que, L., Jr. *Inorg. Chem.* **2001**, *40*, 3181.
(50) Duda, M.; Pascaly, M.; Krebs, B. *Chem. Commun.*, **1997**, 835.
(51) Jang, Ho, G.; Cox, D. D.; Que, L., Jr. *J. Am. Chem. Soc.* **1991**, *113*, 9200.
(52) White, L. S.; Nilsson, P. V.; Pignolet, L. H.; Que, L., Jr. *J. Am. Chem. Soc.* **1984**, *106*, 8312.
(53) Xu, J-Y.; Astner, J.; Walter, O.; Heinemann, F. W.; Schnieders, D.; Merkel, M.; Krebs, B. *Eur. J. Inorg. Chem.* **2006**, 1601.
(54) Reynolds, M. F.; Costas, M.; Ito, M.; Jo, D.-H.; Tipton, A. A.; Whiting, A. K.; Que, L., Jr. *J. Biol. Inorg. Chem.* **2003**, *8*, 263.
(55) Merkel, M.; Schnieders, D.; Baldeau, S. M.; Krebs, B. *Eur. J. Inorg. Chem.* **2004**, 783.

Table 2. Selected Bond Lengths (Angstroms) and Bond Angles (Degrees) for **2**, **3**, and **5a**

2		**3**		**5a**	
Fe(1)−Cl(1)	2.3105(4)	Fe(1)−Cl(1)	2.2883(13)	Fe(1)−O(1)	1.963(5)
Fe(1)−Cl(2)	2.2722(5)	Fe(1)−Cl(2)	2.3195(12)	Fe(1)−O(2)	1.933(5)
Fe(1)−N(1)	2.1938(11)	Fe(1)−Cl(3)	2.3029(13)	Fe(1)−O(3)	2.030(5)
Fe(1)−N(2)	2.2405(16)	Fe(1)−N(1)	2.1762(4)	Fe(1)−N(1)	2.139(6)
		Fe(1)−N(2)	2.2587(3)	Fe(1)−N(2)	2.245(6)
		Fe(1)−N(3)	2.2032(4)	Fe(1)−N(3)	2.172(6)
Cl(1)−Fe(1)−Cl(2)	97.48(14)	Cl(1)−Fe(1)−Cl(2)	97.92(5)	O(1)−Fe(1)−O(2)	82.6(2)
Cl(1)−Fe(1)−N(1)	90.01(3)	Cl(1)−Fe(1)−Cl(3)	94.32(5)	O(1)−Fe(1)−O(3)	108.5(2)
Cl(1)−Fe(1)−N(2)	89.80(3)	Cl(1)−Fe(1)−N(1)	86.19(10)	O(1)−Fe(1)−N(1)	164.9(2)
Cl(1)−Fe(1)−Cl(1a)	101.45(19)	Cl(1)−Fe(1)−N(2)	97.28(10)	O(1)−Fe(1)−N(2)	91.1(2)
Cl(1)−Fe(1)−N(1a)	162.93(3)	Cl(1)−Fe(1)−N(3)	170.22(10)	O(1)−Fe(1)−N(3)	88.2(2)
Cl(2)−Fe(1)−N(1)	93.47(3)	Cl(2)−Fe(1)−Cl(3)	99.27(5)	O(2)−Fe(1)−O(3)	98.2(2)
Cl(2)−Fe(1)−N(2)	168.46(4)	Cl(2)−Fe(1)−N(1)	92.11(10)	O(2)−Fe(1)−N(1)	91.0(2)
Cl(1a)−Fe(1)−Cl(2)	97.48(14)	Cl(2)−Fe(1)−N(2)	160.30(10)	O(2)−Fe(1)−N(2)	104.1(2)
Cl(2)−Fe(1)−N(1a)	93.47(3)	Cl(2)−Fe(1)−N(3)	90.66(10)	O(2)−Fe(1)−N(3)	170.8(2)
N(1)−Fe(1)−N(2)	77.51(4)	Cl(3)−Fe(1)−N(1)	168.42(11)	O(3)−Fe(1)−N(1)	85.9(2)
Cl(1a)−Fe(1)−N(1)	162.93(3)	Cl(3)−Fe(1)−N(2)	92.00(10)	O(3)−Fe(1)−N(2)	152.0(2)
N(1)−Fe(1)−N(1a)	76.25(6)	Cl(3)−Fe(1)−N(3)	88.91(10)	O(3)−Fe(1)−N(3)	84.6(2)
Cl(1a)−Fe(1)−N(2)	89.80(3)	N(1)−Fe(1)−N(2)	76.47(13)	N(1)−Fe(1)−N(2)	77.2(2)
N(1a)−Fe(1)−N(2)	77.51(4)	N(1)−Fe(1)−N(3)	88.81(14)	N(1)−Fe(1)−N(3)	98.0(2)
Cl(1a)−Fe(1)−N(1a)	90.01(3)	N(2)−Fe(1)−N(3)	73.34(13)	N(2)−Fe(1)−N(3)	76.0(2)

Table 3. Electronic Spectral Data (λ_{max} in nm, ϵ_{max} in M^{-1} cm^{-1} in Parenthesis) for Iron(III) Complexes[a] and Their Adducts in Dichloromethane Solution

added ligand[b]	$[Fe(L1)Cl_3]$	$[Fe(L2)Cl_3]$	$[Fe(L3)Cl_3]$	$[Fe(L4)Cl_3]$	$[Fe(L5)Cl_3]$	$[Fe(L6)Cl_3]$	$[Fe(L7)Cl_3]$
none	380 (3700) 290 (7150) 255 (13 880)	384 (2850) 288 (2940) 255 (8040)	388 (4500) 291 (7640) 253 (14 835)	388 (4855) 299 (7840)	357 (4735) 309 (6305) 253 (11 050)	405 (4100) 356 (6630) 317 (13 600)	358 (5320) 310 (7070) 252 (12 840)
H_2DBC [c]	820 (3260) 505 (1970)	848 (1970) 508 (1240)	852 (2700) 512 (1753)	852 (3290) 519 (2160)	856 (1430) 519 (1095)	856 (2380) 531 (1740)	859 (1440) 523 (1040)
H_2DBC [d]	839 (2650) 549 (2170)	737 (2430) 607 (1870)	795 (2710) 619 (1940)	893 (2000) 581 (1500)	899 (1830) 585 (1550)	910 (2600) 588 (1820)	942 (1820) 605 (1830)
3-Me−H_2CAT [c]	790 (2720) 493 (1790)	793 (1595) 502 (1155)	806 (1995) 508 (1475)	807 (2375) 510 (1785)	817 (1665) 515 (1230)	785 (1440) 521 (1380)	816 (1840) 514 (1410)
H_2CAT [c]	760 (2930) 465 (1880)	774 (1280) 486 (1290)	785 (2110) 475 (1560)	789 (2010) 490 (1030)	793 (1715) 482 (1245)	766 (1350) 515 (915)	802 (1915) 481 (1465)
H_2TCC [c]	700 (2970) 475 (1800)	696 (1470) 501 (1030)	719 (2845) 482 (1735)	719 (1940) 508 (1055)	731 (2390) [e] 487 (1510)	692 (1145) 508 (1865)	731 (2630) 487 (1750)

[a] Concentration of the iron(III) complexes, 2×10^{-4} M. [b] The ratio of added ligand to iron(III) complexes was 1:1; the anions were generated by adding 2 equiv of triethylamine. [c] H_2DBC = 3,5-di-*tert*-butylcatechol; 3-Me−H_2CAT = 3-methylcatechol; H_2CAT = catechol; H_2TCC = 3,4,5,6-tetrachlorocatechol. [d] Coordinated chloride ions are removed by treatment with silver perchlorate monohydrate in acetonitrile solution. [e] In agreement with the data (766 nm, 3220 M^{-1} cm^{-1}; 508 nm, 2270 M^{-1} cm^{-1}) for **5a** dissolved in DCM.

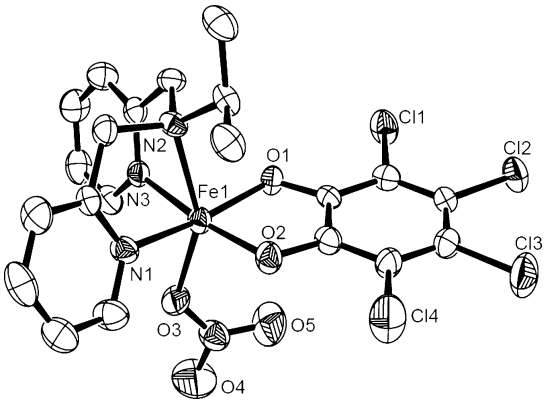

Figure 3. ORTEP diagram of **5a** showing 50% probability thermal ellipsoids and the labeling scheme for selected atoms. All of the hydrogen atoms are omitted for clarity.

induce asymmetry in the catechol binding of the enzymes.[5] Such asymmetric chelation of catechol substrates accounts for the reactivity of the enzymes[54,56] by facilitating dissociation of the longer $Fe-O_{cat}$ bond, to result in monodentatively coordinated catecholate adduct.

Electronic Absorption Spectra. Two visible bands (465−530 and 690−860 nm, Table 3) appear on adding catechols, pretreated with 2 equiv of Et_3N, to iron(III) complexes **1**−**7** in DCM solution. They are attributed to catecholate-to-iron(III) LMCT transitions involving two different catecholate frontier orbitals and the dπ* orbital of iron(III) (Figure 4) and are typical[11−16] of bidentate coordination of the catecholate dianion. The positions of both the low- and high-energy bands depend on the nature of the subtituents on the catecholate ring and are shifted to higher energies when the subtituents are varied from electron-donating to electron-withdrawing (Scheme 3). Thus the 3,5-di-*tert*-butylcatecholate (DBC^{2-}) adducts of iron(III) complexes absorb at energies lower than the other catecholate adducts. For the adducts [Fe(L)(DBC)(Cl)] generated in DCM, both the low- and high-energy LMCT bands exhibit remarkable dependence on the *N*-alkyl substituent in the 3N ligand, and their energies decrease in the order: **1** > **2** > **3** ≥ **4** > **5** ≥ **6** >

(56) Vaillancourt, F. H.; Barbosa, C. J.; Spiro, T. G.; Bolin, J. T.; Blades, M. W.; Turner, R. F. B.; Eltis, L. D. *J. Am. Chem. Soc.* **2002**, *124*, 2485.

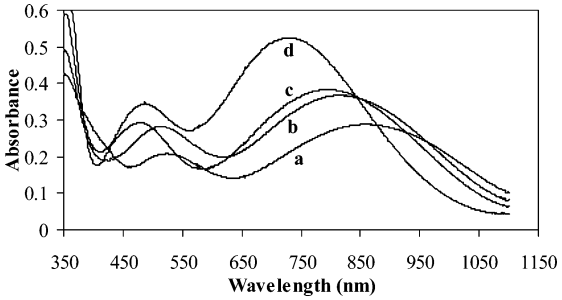

Figure 4. Electronic absorption spectra of adducts of **7** (2×10^{-4} M) generated in situ by adding equimolar amounts of various catecholate dianions in DCM solution: [Fe(L7)(DBC)Cl] (**a**), [Fe(L7)(3Me-CAT)Cl] (**b**), [Fe(L7)(CAT)Cl] (**c**), [Fe(L7)(TCC)Cl] (**d**).

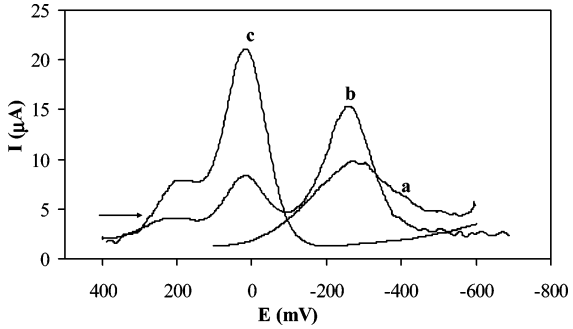

Figure 5. Differential pulse voltammograms of 1 mM [Fe(L4)Cl_3] **4** (a), with 1 mM H_2DBC added (b), and 1 mM H_2DBC and 2 mM triethylamine added (c) in DCM solution at 25 °C. Supporting electrolyte: 0.1 M TBAP. Scan rate: 5 mV s^{-1}.

7 and a similar variation in band energies is observed for the other catecholate adducts also. The decrease in energies of the bands reflects the increase in Lewis acidity of the iron(III) center along the above series, as modified by the *N*-alkyl groups. Thus, upon replacing the −NH hydrogen in **1** by the sterically demanding *N*-methyl group to obtain **2**, the Fe−N_{amine} bond distance increases because the lone-pair orbital on the secondary nitrogen atom is not oriented exactly toward the iron(III) orbital. This causes the negative charge built on iron(III) to decrease, and as a result the dπ* orbitals of iron(III) are stabilized, leading to a decrease in energy gap[57] between the dπ* orbital and ligand catecholate orbitals and hence the observed decrease in the catecholate-to-iron(III) LMCT band energy. A similar increase in the Fe−N_{amine} bond distance and shifts in both low- and high-energy bands to lower energies are observed upon replacing the *N*-methyl group in **2** with the *N*-*n*-propyl group as in **3**. Thus, the increase in steric demand along the above series leads to an increase in positive charge on iron(III) and hence a stronger interaction of catecholates with an iron(III) center.

Further, upon removing the coordinated chloride ions by treating **1**−**7** in DCM with 3 equiv of $AgClO_4 \cdot H_2O$ (CH_3CN) and then adding 1 equiv of DBC^{2-} to generate $[Fe(L)(DBC)(Sol)]^+$ species (Sol = H_2O/CH_3CN), both the high- and the low-energy bands are shifted significantly (20−110 nm) to lower energies for all of the complexes, with the exception of $[Fe(L2)(DBC)(Sol)]^+$ and $[Fe(L3)(DBC)(Sol)]^+$, suggesting an increase in Lewis acidity of the iron(III) center and hence a stronger iron(III)-catecholate interaction (cf. above). The enhancement in covalency of the iron−catecholate bond leads to stabilization of the semiquinone radical character[58] of bound DBC^{2-} (cf. below). Also, for the $[Fe(L)(DBC)(Sol)]^+$ species, the low-energy LMCT band varies (40−83 nm) as **2** > **3** > **4** > **5** > **6** > **7** depending upon the steric bulk of *N*-alkyl groups. This illustrates that upon increasing the length of the *N*-alkyl group and the degree of substitution at the α-carbon atom of the *N*-methyl group in $[Fe(L2)(DBC)(Sol)]^+$ and upon incorporation of the methyl group at the β-carbon atom as in **4**, the Lewis acidity of the iron(III) center increases, rendering the binding of DBC^{2-} stronger. Similar variation (44−107 nm) in the high-energy LMCT band is observed for the DBC^{2-} adducts of **1** and **4**−**7**, but not for those of **2** and **3**.

Electrochemical Behavior. The electrochemical features of the iron(III) complexes and their DBC^{2-} adducts generated in situ were investigated in DCM solution by employing cyclic (CV) and differential pulse voltammetry (DPV) on a stationary platinum-sphere electrode. Iron(III) complexes **1**−**3**, **5**, and **6** exhibit a coupled pair of redox waves at negative potentials, which are assigned[11,15] to Fe^{III}/Fe^{II} couple (Figure 5and S1, S3, and S4 in the Supporting Information; Table 4), whereas **4** and **7** exhibit only a cathodic wave. The $E_{1/2}$ values of Fe^{III}/Fe^{II} redox potentials follow the trend **1** > **2** > **3** > **4** < **5** > **6** ≈ **7**, reflecting a decrease in Lewis acidity of the iron(III) center along this series. This trend is in contrast to that observed above, obviously because the coordinated chloride ions compensate for the increase in the positive charge on iron effected by the sterically hindering *N*-alkyl groups. On adding 1 equiv of H_2DBC to **1**−**7** in DCM solution, a new wave appears in the CV and DPV responses (Figures 5), which corresponds to DBSQ/DBC^{2-} couple[11−15,52,59] of [Fe(L)(DBC)(Cl)] species generated. On adding 2 equiv of Et_3N to deprotonate the catechol, the reduction current of this couple increases and the Fe^{III}/Fe^{II} redox wave tends to vanish completely (Figures 5), which is expected[11−15,52,57,59] to be shifted to a more-negative potential due to the chelation of DBC^{2-}. Also, the redox potential of the DBSQ/DBC^{2-} couple of the [Fe(L)(DBC)(Cl)] species is observed in the range −0.075 to −0.009 V (Table 4), which is less negative than that of the free DBSQ/DBC^{2-} couple (E_{pc}, −1.34 V vs SCE).[60] This confirms the enhanced covalency of iron−catecholate interaction and stabilization of the semiquinone radical of the coordinated DBC^{2-} anion toward oxidation and is consistent with the above spectral results.

The Fe^{III}/Fe^{II} redox waves of the $[Fe(L)(Sol)_3]^{3+}$ species, generated in DCM by treating **1**−**7** with 3 equiv of $AgClO_4 \cdot H_2O$ (CH_3CN), are shifted to potentials enormously more positive (0.412−0.480 V, Figure 6, S2 in the Supporting Information, and Table 4) than those observed for the corresponding [Fe(L)Cl_3] complexes, as expected, and the

(57) Cox, D. D.; Que, L., Jr. *J. Am. Chem. Soc.* **1988**, *110*, 8085.
(58) Funabiki, T.; Fukui, A.; Hitomi, Y.; Higuchi, M.; Yamamoto, T.; Tanaka, T.; Tani, F.; Naruta, Y. *J. Inorg. Biochem.* **2002**, *91*, 151.
(59) Viswanathan, R.; Palaniandavar, M. *J. Chem. Soc., Dalton Trans.* **1995**, 1259.
(60) Nanni, E. J.; Stallings, M. D.; Sawyer, D. T. *J. Am. Chem. Soc.* **1980**, *102*, 4481.

Table 4. Electrochemical Data[a] for $[Fe(L)Cl_3]$, $[Fe(L)(DBC)Cl]$,[b] $[Fe(L)(Sol)_3]^{3+}$ [c], and $[Fe(L)(DBC)(Sol)]^+$ [d] in Dichloromethane at 25.0 ± 0.2 °C at a Scan Rate of 50 mV s^{-1} (CV) and 5 mV s^{-1} (DPV)

	$E_{1/2}$ (V)			$E_{1/2}$ (V)		
complexes	CV	DPV	complexes	CV	DPV	redox process
$[Fe(L1)Cl_3]$	−0.188	−0.206	$[Fe(L1)(Sol)_3]^{3+}$	0.165	0.157	$Fe^{III} \rightarrow Fe^{II}$
+ H_2DBC	−0.080	−0.095	+ H_2DBC	0.317	0.321	DBSQ → DBC
$[Fe(L1)(DBC)Cl]$	−0.231	−0.227		0.115	0.131	$Fe^{III} \rightarrow Fe^{II}$
			$[Fe(L1)(DBC)(Sol)]^+$	0.492	0.503	DBQ → DBSQ
	−0.098	−0.075			0.313	DBSQ → DBC
				0.117	0.151	$Fe^{III} \rightarrow Fe^{II}$
$[Fe(L2)Cl_3]$	−0.250	−0.257	$[Fe(L2)(Sol)_3]^{3+}$	0.188	0.209	$Fe^{III} \rightarrow Fe^{II}$
+ H_2DBC	−0.031	−0.055	+ H_2DBC	0.427	0.429	DBSQ → DBC
	−0.240	−0.208		0.166	0.177	$Fe^{III} \rightarrow Fe^{II}$
$[Fe(L2)(DBC)Cl]$	−0.041	−0.023	$[Fe(L2)(DBC)(Sol)]^+$	0.375	0.407	DBSQ → DBC
				0.149	0.167	$Fe^{III} \rightarrow Fe^{II}$
				−0.014	−0.015	$Fe^{III} \rightarrow Fe^{II}$
$[Fe(L3)Cl_3]$	−0.294	−0.287	$[Fe(L3)(Sol)_3]^{3+}$	0.125	0.125	$Fe^{III} \rightarrow Fe^{II}$
+ H_2DBC	−0.033	−0.039	+ H_2DBC	0.422	0.413	DBSQ → DBC
	−0.293	−0.289		0.095	0.081	$Fe^{III} \rightarrow Fe^{II}$
$[Fe(L3)(DBC)Cl]$	−0.061	−0.045	$[Fe(L3)(DBC)(Sol)]^+$	0.427	0.413	DBSQ → DBC
				0.097	0.134	$Fe^{III} \rightarrow Fe^{II}$
$[Fe(L4)Cl_3]$		−0.299	$[Fe(L4)(Sol)_3]^{3+}$	0.186	0.181	$Fe^{III} \rightarrow Fe^{II}$
+ H_2DBC	0.133	0.181	+ H_2DBC			DBQ → DBSQ
	0.004	−0.009		0.443	0.441	DBSQ → DBC
	−0.270	−0.285		0.187	0.187	$Fe^{III} \rightarrow Fe^{II}$
$[Fe(L4)(DBC)Cl]$	0.154	0.161	$[Fe(L4)(DBC)(Sol)]^+$			DBQ → DBSQ
	−0.014	−0.009		0.387	0.415	DBSQ → DBC
				0.154	0.165	$Fe^{III} \rightarrow Fe^{II}$
				0.008	−0.017	$Fe^{III} \rightarrow Fe^{II}$
$[Fe(L5)Cl_3]$	−0.290	−0.28	$[Fe(L5)(Sol)_3]^{3+}$	0.152	0.157	$Fe^{III} \rightarrow Fe^{II}$
+ H_2DBC	0.178	0.213	+ H_2DBC			DBQ → DBSQ
	−0.024	−0.021		0.446	0.445	DBSQ → DBC
	−0.268	−0.271		0.161	0.157	$Fe^{III} \rightarrow Fe^{II}$
$[Fe(L5)(DBC)Cl]$	0.186	0.193	$[Fe(L5)(DBC)(Sol)]^+$			DBQ → DBSQ
	−0.036	−0.019		0.400	0.415	DBSQ → DBC
				0.178	0.213	$Fe^{III} \rightarrow Fe^{II}$
				−0.064	−0.047	$Fe^{III} \rightarrow Fe^{II}$
$[Fe(L6)Cl_3]$	−0.333	−0.323	$[Fe(L6)(Sol)_3]^{3+}$	0.146	0.139	$Fe^{III} \rightarrow Fe^{II}$
+ H_2DBC	−0.058	−0.045	+ H_2DBC			DBSQ → DBC
	−0.297	−0.291				$Fe^{III} \rightarrow Fe^{II}$
	0.057	0.057	$[Fe(L6)(DBC)(Sol)]^+$			DBQ → DBSQ
$[Fe(L6)(DBC)Cl]$	−0.057	−0.051		0.393	0.411	DBSQ → DBC
				0.169	0.207	$Fe^{III} \rightarrow Fe^{II}$
$[Fe(L7)Cl_3]$		−0.324	$[Fe(L7)(Sol)_3]^{3+}$	0.126	0.125	$Fe^{III} \rightarrow Fe^{II}$
+ H_2DBC	0.173	0.213	+ H_2DBC			DBQ → DBSQ
	−0.018	−0.021				DBSQ → DBC
	−0.313	−0.309				$Fe^{III} \rightarrow Fe^{II}$
$[Fe(L7)(DBC)Cl]$	0.169	0.183	$[Fe(L7)(DBC)(Sol)]^+$			DBQ → DBSQ
	−0.042	−0.039				DBSQ → DBC

[a] Potential measured versus $Ag(s)/Ag^+$ (0.01 M, 0.10 M TBAP); add 0.544 V to convert to NHE. [b] Generated by adding 1 equiv of H_2DBC and 2 equiv of triethylamine to complex $[Fe(L)Cl_3]$. [c] Coordinated chloride ions are removed by treatment with 3 equiv of silver perchlorate monohydrate in acetonitrile solution. [d] Generated by adding 1 equiv of H_2DBC and 2 equiv of triethylamine to complex $[Fe(L)(Sol)_3]^{3+}$.

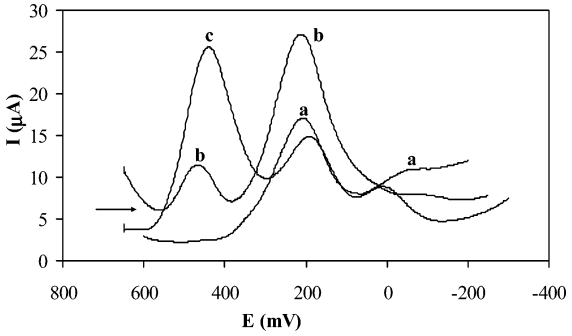

Figure 6. Differential pulse voltammograms of 1 mM $[Fe(L4)Cl_3]$ after treatment with 3 equiv of $AgClO_4 \cdot H_2O$ (a), with 1 mM H_2DBC added (b), and 1 mM H_2DBC and 2 mM triethylamine added (c) in DCM solution at 25 °C. Supporting electrolyte: 0.1 M TBAP. Scan rate: 5 mV s^{-1}.

$E_{1/2}$ values follow a trend, which is almost the same as that observed for the chloro complexes. On adding 1 equiv of H_2DBC to the solvated complexes to generate the $[Fe(L)(DBC)(Sol)]^+$ species, a new wave corresponding to the $DBSQ/DBC^{2-}$ couple appears. On adding 2 equiv of Et_3N, the reduction current of $DBSQ/DBC^{2-}$ redox couple increases, whereas that of the Fe^{III}/Fe^{II} couple decreases. The appearance of the $DBSQ/DBC^{2-}$ couple of the $[Fe(L)(DBC)(Sol)]^+$ species, except $[Fe(L1)(DBC)(Sol)]^+$ (0.321 V), at potentials (∼ 0.410 V) more positive than those of the $[Fe(L)(DBC)(Cl)]$ species reveals that the semiquinone radical character of coordinated DBC^{2-} in the former is much more stabilized (more reactive) toward oxidation than that in the latter. It is remarkable that the stabilization of the catecholate oxidation state (∼400 mV) in these adducts is higher than that for the adducts of chloro complexes. This means that the electron transfer[61] from catecholate adducts to dioxygen is thermodynamically unfavorable more in solvated complexes than in chloro complexes, obviously due to the higher

(61) Kovaleva, E. G.; Lipscomb, J. D. *Science* **2007**, *316*, 453.

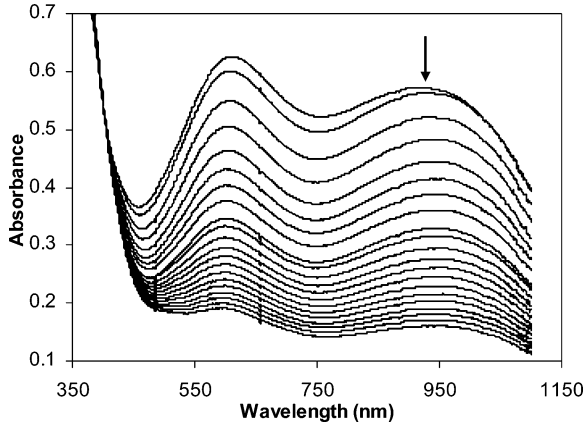

Figure 7. Progress of the reaction of adduct $[Fe(L7)(DBC)(Sol)]^+$ with O_2 in DCM solution. The disappearance of the DBC^{2-}-to-iron(III) charge-transfer band is monitored.

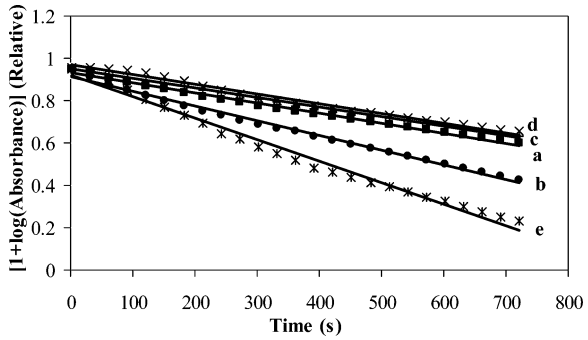

Figure 8. Plots of [1 + log(Absorbance)] versus time for the reaction of $[Fe(L)(DBC)(Sol)]^+$ with O_2 at 25 °C in DCM solution. Concentration of complexes, 4×10^{-4} M (**a**): $[Fe(L2)(DBC)(Sol)]^+$, (**b**): $[Fe(L4)(DBC)(Sol)]^+$, (**c**): $[Fe(L5)(DBC)(Sol)]^+$, (**d**): $[Fe(L6)(DBC)(Sol)]^+$, (**e**): $[Fe(L7)(DBC)(Sol)]^+$.

Lewis acidity of iron(III) centers. But, interestingly, it reacts with dioxygen (cf. below). The Fe^{III}/Fe^{II} reduction wave of the $[Fe(L)(DBC)(Sol)]^+$ species is discerned in the range −0.047 to −0.015 V due to the chelation of DBC^{2-}.

Dioxygenase Activity. The catecholate adducts [Fe(L)-(DBC)(Cl)] and $[Fe(L)(DBC)(Sol)]^+$ were generated in situ by treating respectively the complexes $[Fe(L)Cl_3]$ and $[Fe(L)(Sol)_3]^{3+}$ with equimolar quantities of H_2DBC and 2 equiv of Et_3N in DMF and DCM solvents and then exposed to molecular oxygen. The disappearance of the lower-energy catecholate-to-iron(III) LMCT band (Figures 7and S5 in the Supporting Information) on oxygenation exhibits pseudo-first-order kinetics, as judged from the linearity of the plot [1 + log(Absorbance)] versus time (Figure 8), and the values of k_{obs} were obtained from the slopes of these plots. Only very small changes in the values of k_{obs} are observed when the concentration of $[Fe(L)(DBC)(Sol)]^+$ is varied from 2×10^{-4} to 5×10^{-4} M. The second-order rate constants were calculated[62,63] (Table 5) using the equation,

$$k_{O_2} = k_{obs}/[O_2]$$

The products of the cleavage of H_2DBC in DCM solvent (Table 5) are identified (**8**−**13**, Scheme 4) by GC-MS and ^1H NMR techniques and quantified by GC analysis.

We have previously observed the exclusive formation of intradiol cleavage products for **1** and other similar complexes of linear tridentate 3N ligands in DMF solvent.[15] The catecholate adducts of these complexes in DMF appear to rearrange in solution to a species with meridional coordination of the 3N ligand, which facilitates intradiol rather than extradiol cleavage.[15] All of the present complexes also afford major amounts of intradiol cleavage products and smaller amounts of extradiol (1.5−5%) products in DMF solvent. On the other hand, extradiol cleavage products are isolated in 13−22% yield (the results are not shown here) for the adducts $[Fe(L)(DBC)(Sol)]^+$ generated in DMF. It is clear that the presence of a vacant or solvent-coordinated site on the iron(III) center of the catecholate adducts is essential for dioxygen attack to achieve extradiol cleavage products[27,64] and that a coordinated chloride ion in the adduct [Fe(L)-(DBC)Cl] is difficult to be replaced by dioxygen to afford extradiol cleavage products. Also, all of the [Fe(L)(DBC)-Cl] complexes show lower reactivity in DCM solvent, and the cleavage products observed are less than 1%, even after 2 days of reaction under oxygen atmosphere. This illustrates that the strongly coordinated chloride ion (cf. conductivity studies) in these complexes is difficult to be replaced in DCM much more than in DMF. Thus, it is remarkable that all of the solvent-coordinated adducts $[Fe(L)(DBC)(Sol)]^+$ generated in DCM solvent show enhanced yields of extradiol cleavage products (26.7−68.0%, Table 5). Further, the catecholate adducts derived from **4**−**6** show the highest yield of extradiol cleavage products (59.5−68.0%), with the extradiol-to-intradiol cleavage product selectivity (*E*/*I*) being approximately 6:1, whereas the adduct derived from **3** shows a lower selectivity (*E*/*I*, 4:1). On the other hand, the adducts derived from **1**, **2**, and **7** show 26.7−38.7% of extradiol cleavage products with much lower selectivity (*E*/*I*, ∼1:1). So, it is clear that the bulkiness of the *N*-alkyl groups of the linear 3N ligands dictate the regioselective formation of cleavage products.

Bugg and co-workers[64] have ruled out the formation of the dioxetane intermediate proposed in the molecular oxygen activation (extradiol cleavage) as well as in the substrate activation (intradiol cleavage) mechanisms and proposed that cyclohexadienyl peroxide is the common intermediate formed in both of these mechanisms. The cis-facially coordinated 3N ligands in the present complexes allow the two reactants (molecular oxygen and catechol) to occupy the opposite face of the iron coordination sphere thereby bringing them in close proximity and in the proper orientation to form the cyclohexadienyl peroxide intermediate,[65] which on alkenyl migration gives extradiol cleavage products and on acyl migration yields intradiol cleavage products. So, it emerges from the present study that the *N*-alkyl groups *n*-propyl, iso-butyl, iso-propyl, and cyclohexyl in the 3N ligand complexes facilitate

(62) Mialane, P.; Tehertanov, L.; Banse, F.; Sainton, J.; Girerd, J. *Inorg. Chem.* **2000**, *39*, 2440.
(63) Yamahara, R.; Ogo, S.; Watanabe, Y.; Funabiki, T. *Inorg. Chim. Acta* **2000**, *300*−*302*, 587.
(64) Bugg, T. D. H.; Lin, G. *Chem. Commun.* **2001**, *11*, 941.
(65) Barbaro, P.; Bianchini, C.; Mealli, C.; Meli, A. *J. Am. Chem. Soc.* **1991**, *113*, 3181.

Table 5. Kinetic Data[a] for Oxidative Cleavage of H_2DBC Catalyzed by Iron(III) Complexes in DMF and DCM and the Cleavage Products **8**−**13** (Scheme 4)

	Complex + 3 $AgClO_4 \cdot H_2O$			Cleavage products in %	
complex	k_{O_2} (10^{-3} $M^{-1}s^{-1}$) in DMF	k_{O_2} (10^{-2} $M^{-1}s^{-1}$) in DMF	k_{O_2} ($M^{-1}s^{-1}$) in DCM	extradiol	intradiol
[Fe(L1)Cl_3]	17.00 ± 0.3	4.08 ± 0.14	0.162 ± 0.08	5.8 (**9**) 20.1 (**11**) 0.8 (**10**)	18.6 (**13**)
[Fe(L2)Cl_3]	3.10 ± 0.1	1.01 ± 0.02	0.152 ± 0.03	6.1 (**9**) 2.5 (**8**) 15.3 (**11**) 14.8 (**10**)	24.5 (**13**) 16.5 (**12**)
[Fe(L3)Cl_3]	1.65 ± 0.02	1.24 ± 0.05	0.159 ± 0.03	8.4 (**9**) 29.4 (**11**)	11.7 (**13**)
[Fe(L4)Cl_3]	2.83 ± 0.5	0.85 ± 0.03	0.311 ± 0.08	12.4 (**9**) 47.1 (**11**)	14.4 (**13**)
[Fe(L5)Cl_3]	1.94 ± 0.4	1.39 ± 0.04	0.188 ± 0.08	16.8 (**9**) 46.1 (**11**) 5.1 (**10**)	11.1 (**13**)
[Fe(L6)Cl_3]	3.74 ± 0.3	0.96 ± 0.04	0.194 ± 0.01	16.1 (**9**) 44.7 (**11**) 3.3 (**10**)	12.8 (**13**)
[Fe(L7)Cl_3]	2.82 ± 0.3	3.03 ± 0.10	0.376 ± 0.04	7.9 (**9**) 26.9 (**11**)	27.5 (**13**)

[a] $k_{O_2} = k_{obs}/[O_2]$. The solubility of O_2 in DMF is accepted to be 4.86 mM; in DCM, 5.80 mM at 25 °C. The kinetic data were obtained by monitoring the disappearance of the lower-energy DBC^{2-}-to-iron(III) LMCT band.

Scheme 4. Products of Catechol Cleavage of H_2DBC Mediated by [Fe(L)Cl_3)] Complexes Using Molecular Oxygen: 4,6-Di-*tert*-butyloxepine-2,3-dione (**8**), 3,5-Di-*tert*-butyl-2-pyrone (**9**), 5,7-Di-*tert*-butyloxepine-2,3-dione (**10**), 4,6-Di-*tert*-butyl-2-pyrone (**11**), 3,5-Di-*tert*-butyl-1-oxacyclohepta-3,5-diene-2,7-dione (**12**), 3,5-Di-*tert*-butyl-5-(carboxymethyl)-2-furanone (**13**)

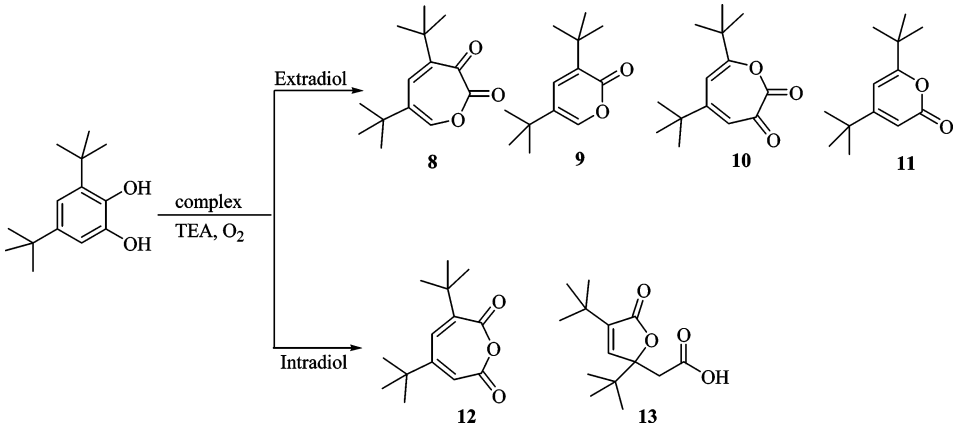

alkenyl migration, whereas the parent ligand, methyl, and *tert*-butyl groups favor both alkenyl and acyl migrations (Scheme 5), leading to regioselectivity of the cleavage. Thus, the Fe−O_{cat} bonds in the former complexes become different in length (cf. above) and render the complex reactive.[52,57] The longer Fe−O_{cat} bond would dissociate, leading to monodentate coordination of catechol, which has been proposed[27] to facilitate extradiol cleavage. Also, the *N*-alkyl groups will be oriented away from the sp^3-hybridized carbon atom of the catecholate substrate in the intermediate, facilitating alkenyl migration and, hence, formation of enhanced extradiol cleavage products. On the other hand, the bulky *N*-*tert*-butyl group in [Fe(L7)(DBC)(Sol)]$^+$ favors both of the migrations equally, thus explaining the observed *E/I* value of 1:1. For the [Fe(L3)(DBC)(Sol)]$^+$ adduct with the less sterically hindered *N*-propyl group, lower amounts of extradiol cleavage products (*E/I*, 4:1) are observed.

The second-order reaction rate constants (k_{O_2}, 0.85−4.08 × 10^{-2} M^{-1} s^{-1}, Table 5) for [Fe(L)(DBC)(Sol)]$^+$ adducts derived from **1**−**7** in DMF are 5−10 fold higher than those (0.17−1.70 × 10^{-2} M^{-1} s^{-1}) for [Fe(L)(DBC)(Cl)] adducts in the same solvent. This is expected of the higher Lewis acidity[31,57] of the iron(III) center in [Fe(L)(DBC)(Sol)]$^+$ adducts, which favors catecholate and dioxygen binding. Upon introducing bulky alkyl groups near the donor atoms in the heterocyclic ring systems[16,48] as in [Fe(Tp^{ipr,tBu})(DBC)]$^+$ and [Fe(6-MeTPA)(DBC)]$^+$, catechol and dioxygen are discouraged from binding to the iron(III) center, leading to a decrease in dioxygenase activity of the complexes. On the other hand, dioxygen could approach the iron(III) center of the present [Fe(L)(DBC)(Sol)]$^+$ adducts opposite to the sterically hindered *N*-alkyl groups (cf. crystal structure of **5a**). Further, interestingly, the reaction rates for [Fe(L)(DBC)(Sol)]$^+$ complexes in DCM are 10−130 fold higher than those in DMF solvent. Obviously, the displacement of coordinated H_2O/CH_3CN in the adduct by dioxygen in DMF solution is more facile than that of the solvent by dioxygen in the non-coordinating solvent DCM.

Scheme 5. Proposed Mechanism for Both Intra- and Extradiol Cleavage Pathway

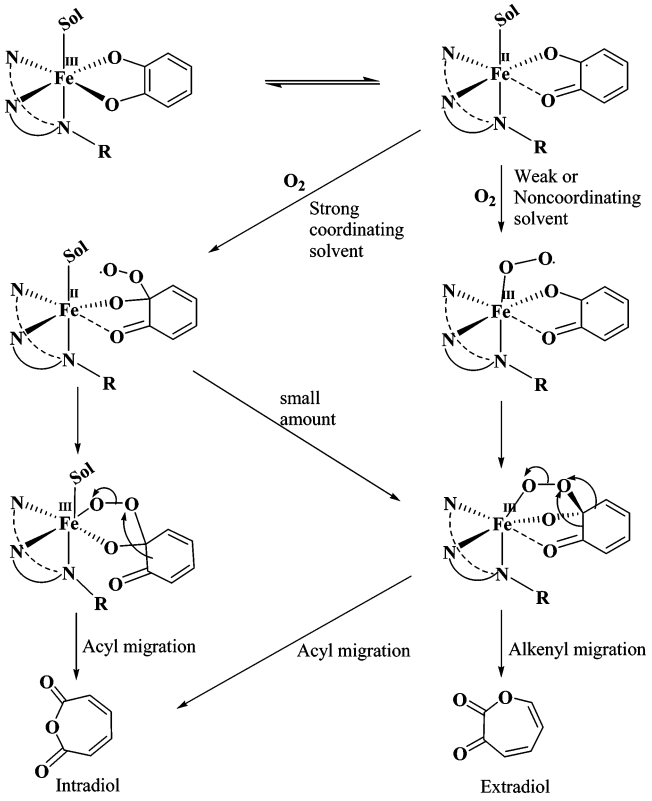

The plot of log (k_{O_2}) versus energy of the low-energy catecholate-to-metal CT band (Figure 9) is linear, which is in line with the trend in Lewis acidity of iron(III) centers (cf. above). The adducts [Fe(L4)(DBC)(Sol)]$^+$ and [Fe(L7)(DBC)(Sol)]$^+$ exhibit a positive deviation from the straight line, illustrating that in addition to the high Lewis acidity of iron(III) centers the bulkiness and orientation of *N*-alkyl groups of the adducts enhance the reaction rate (cf. above).[66,67] Very recently, Funabiki et al. have observed[68] a similar linear correlation for the reaction of [Fe(TPA)(R-Cat)]BPh_4 adducts, where R-Cat are differently substituted catechols with O_2 and used a spin-inversion phenomenon to illustrate the LMCT energy-dependent reactivity. The reactivity of the present adducts is accounted for by invoking a two-state reaction pathway, which involves a spin-inversion process from the spin-quartet state ($S = {}^5/_2$) in (L)$Fe^{III}-Cat^{2-}$ to the upper-lying spin-singlet ($S = {}^1/_2$) state in (L)$Fe^{II}-SQ$, upon O_2 approching the iron(III) center. As O_2 approaches the iron(III)-catecholate adduct, the ligand field strength increases, causing spin-pairing leading to spin-inversion and formation of Fe(II)−SQ state. Thus, in the case of [Fe(L7)(DBC)(Sol)]$^+$ with R = *tert*-butyl group, the approach of O_2 takes place on the face opposite to the *N*-alkyl group and as the sterically hindering *tert*-butyl group leads to the strongest iron(III)-catecholate interaction facilitating the formation of the upper lying (L)Fe(II)−SQ spin state, which is primed to react with

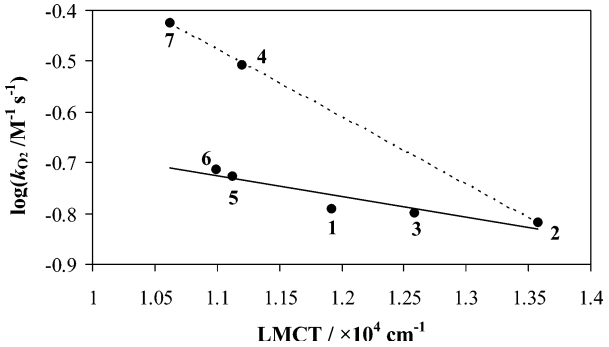

Figure 9. Plot of the logarithm of the second-order reaction rate constant versus the energy of the lower-energy LMCT band of [Fe(L)(DBC)(Sol)]$^+$ derived from **1**−**7** in DCM solution.

O_2 and hence the highest rate observed. In this regard, it is interesting to note that for the redox couple DBSQ/DBC^{2-}, which involves the spin-inversion, well-defined reduction and oxidation waves with relatively low ΔE_p values are discerned for all of the adducts in the cyclic voltammetric experiment, and this supports the involvement of the facile spin-inversion. However, it is to be noted that the $E_{1/2}$ values of DBSQ/DBC^{2-} couples, which represent the Lewis acidity of all of the [Fe(L)(DBC)(Sol)]$^+$ adducts, except [Fe(L1)(DBC)(Sol)]$^+$ possessing a lower positive $E_{1/2}$ value (cf. above), are almost the same in DCM solvent. The energy needed for the spin-inversion corresponds to the LMCT band energy, which is found to vary systematically along the present series of complexes depending upon the *N*-alkyl group. Thus, for the present complexes both the Lewis acidity and the ligand steric demand enhance the reactivity of complexes toward dioxygenation of catechol substrates.

Conclusions

A series of iron(III) complexes of the type [Fe(L)Cl_3], where L is the linear *N*-alkyl-substituted bis(pyrid-2-ylmethyl)amine, have been isolated and studied as structural and functional models for catechol dioxygenase enzymes. The X-ray crystal structures of two of the complexes reveal that the 3N ligands are cis-facially coordinated, and the replacement of *N*-methyl substituent by *N*-*n*-propyl substituent causes the Fe−N_{py}/Fe−Cl bonds to differ in length. Also, the *N*-*iso*-propyl substituent in a tetrachlorocatecholate adduct causes the Fe−O_{cat}/N_{py} bond lengths to differ. Our studies reveal that stereo-electronic factors like the Lewis acidity of the iron(III) center and the steric demand of ligands, as regulated by the *N*-alkyl subtituents, determine the cleavage yields and the rate of dioxygenation in DCM and DMF solvents. It is remarkable that the iron(III)-catecholate adducts with the *N*-alkyl groups *n*-propyl, *iso*-butyl, *iso*-propyl, and cyclohexyl confer enhanced selectivity toward extradiol cleavage, whereas that with a *N*-*tert*-butyl substituent enhances the reaction rate.

Acknowledgment. We sincerely thank the Council of Scientific and Industrial Research, New Delhi, for a Senior Research Fellowship to K.V. We thank Department of Science and Technology, New Delhi, for the Award of

(66) Merkel, M.; Muller, F. K.; Krebs, B. *Inorg. Chim. Acta* **2002**, *337*, 308.
(67) Lipscomb, J. D.; Orville, A. M. *Met. Ions Biol. Syst.* **1992**, *28*, 243.
(68) Hitomi, Y.; Yoshida, M.; Higuchi, M.; Minami, H.; Tanaka, T.; Funabiki, T. *J. Inorg. Biochem.*, **2005**, *99*, 755.

Ramanna Fellowship to M.P and also for supporting this research [Scheme No. SR/S1/IC-45/2003 and SR/S5/BC-05/2006]. We thank Mr. R. Seshagiri for some experimental assistance. We thank Prof. K. Natarajan, Bharathiar University, Coimbatore, for CHN analysis.

Supporting Information Available: Electronic spectra, cyclic voltammograms, differential pulse voltammograms, and crystallographic data in CIF format for **2**, **3**, and **5a**. This material is available free of charge via the Internet at http://pubs.acs.org.

IC700822Y